IEEE Access
Multidisciplinary | Rapid Review | Open Access Journal

Received September 8, 2019, accepted October 1, 2019, date of publication October 8, 2019, date of current version October 23, 2019.

Digital Object Identifier 10.1109/ACCESS.2019.2946302

Design of Dual-Band Bandpass Filter With Simultaneous Narrow- and Wide-Bandwidth and a Wide Stopband

MIN-HANG WENG[1], SIANG-WEN LAN[2], SHOOU-JINN CHANG[2], AND RU-YUAN YANG[3]

[1]School of Information Engineering, Putian University, Putian 351100, China
[2]Institute of Microelectronics and Department of Electrical Engineering, Center for Micro/Nano Science and Technology, Advanced Optoelectronic Technology Center, National Cheng Kung University, Tainan 701, Taiwan
[3]Graduate Institute of Materials Engineering, National Pingtung University of Science and Technology, Pingtung 912, Taiwan

Corresponding author: Ru-Yuan Yang (ryyang@mail.npust.edu.tw)

ABSTRACT This paper presents a novel dual-band bandpass filter with narrow and wide passband simultaneously and a wide stopband. The dual-band bandpass filter is implemented using a stepped-impedance ring loaded resonator (SIRLR). The properties of the SIRLR are analyzed in detail based on the even- and odd-mode equivalent circuits. Resonant modes, excited by SIRLR, can be controlled and used to form a narrow passband at 2.4 GHz with bandwidth ratio of 8% and a wide passband from 3 to 5 GHz, with insertion losses less than 1.5 dB for both two passbands. Three transmission zeros are created near the passband edge to improve the passband selectivity and achieve a sharp cutoff skirt (over 60 dB/GHz). In addition, for wide stopband consideration, rectangular stub loaded resonators (RSLRs) are tapped on the input and output ports of above dual-band filter without destroying the dual-band performances. Thus, the proposed dual-band filter with a wide stopband region from 5 to 20 GHz with a rejection level of 25 dB is also achieved. The measured results show a good agreement with the simulated results.

INDEX TERMS Dual-band, isolation, rectangular stub loaded resonator (RSLR), stepped-impedance ring loaded resonator (SIRLR), stopband.

I. INTRODUCTION

In recent years, for the demand of high-quality service, multi-band mobile equipments have attracted much interest for use in wireless communications applications, such as the Global System for Mobile communications (GSM), IEEE 802.11 wireless local area networks (WLANs) and ultra-wide band (UWB) system. In wireless communication systems, microwave filters are the key elements, because they affect the operation of whole system, pass desired frequency band signal and restrict the unwanted incoming frequency band signal. In addition, microwave filters are generally fabricated by utilizing planar filter process due to low cost and simple fabrication process.

Accordingly, many different schemes had been proposed to construct the planar filters with dual-band characteristics [1]–[15]. For example, a coupled-serial-shunted line structure used to provide a notch at the middle of the passband to realize a dual-band bandpass filter [1]. A dual-band bandpass filter could also be realized by using ring dual-mode resonators, and the resonant characteristics were varies by adopting non-uniform impedance microstrip lines [2]. Dual-path propagation filter by combining two independent resonators was used to excite a dual-band response with a high passband isolation since two passbands could be controlled independently by tuning the physical dimensions of the corresponding resonator [3], [4]. Especially, multi-modes resonators, such as stepped-impedance resonator (SIR) [5]–[10] and stub loaded resonator (SLR) [11]–[15], are most popular to be used to achieve the required dual-band responses. For the SIR, the spurious response could be controlled effectively by tuning the determined ratios (electrical length ratio and impedance ratio). For example, compact and low loss dual-band bandpass filter using pseudo-interdigital stepped impedance resonators for WLANs was presented [7]. The passband frequencies can be adjusted to desirable values, however it is still difficult to control the bandwidths. For the SLR, the spurious response could be adjusted easily by tuning

The associate editor coordinating the review of this manuscript and approving it for publication was Nagendra Prasad Pathak.

the location of the loaded stub. With different numbers and types of the stubs, such as open or short stub, dual-band BPFs based on multi-mode stub-loaded resonators can be designed. In [11]–[13], the first two resonant modes were used to form the first passband, and the third and fourth resonant modes were used to obtain the second passband. Most of the reported works focused on the dual passband with two narrow band responses. Dual-band bandpass filter having narrow-band and wide-band characteristics simultaneously attracted less attention in past. In a previous work [7], a dual-band bandpass filter with narrow-band and wide-band performances was presented. Two SIRs with multi modes were used. Each resonant mode was controlled by determining a proper impedance ratio. Moreover, with proper coupling arrangement, the transmission zeros were provided to enhance the passband isolation between the narrow-band and the wide-band. However, to avoid the interference with other communication systems, a wide stopband design for the filter is always required.

In this design, a novel dual-band bandpass filter having a narrow-band and wide-band response and with an extended stopband is shown. The dual-band responses for WLAN and UWB uses are excited merely by one stepped-impedance ring loaded resonator (SIRLR). Wherein, the SIRLR had been used to design a dual-narrowband bandpass filter [13]. However, the degree of designing freedom is restrained due to each mode of SIRLR is controlled by merely tuning the length of coupling line. In comparison with above mentioned design, we introduced novel ratio parameters, which are related to the physical dimensions of the SIRLR, to control each mode of SIRLR much more accurately. In addition, resonant characteristics of SIRLR was completely analyzed and plotted to increase the degree of designing freedom. Moreover, a wide stopband for the interference suppression can be further achieved by applying a pair of rectangular stub loaded resonator (RSLR) tapped at the input/output ports of the SIRLR.

The design procedure and limitations of the proposed structure are described in detail in the following sections. The organization of this paper is shown as follows. In introduction section, the motivation and novelty of this study are addressed. In section II, the equivalent circuit and the resonant modes of the SIRLR are discussed in detail. By tuning the electrical length ratio and impedance ratio, the resonant modes of the SIRLR can be varied effectively to desired position. Thus a narrow passband at 2.4 GHz with bandwidth ratio of 8% and a wide passband from 3 to 5 GHz can be achieved. In section III, the RSLR is used to obtain a wide stopband, since it a low-pass resonator and can generate several transmission zeros at the desired locations. In this section, the equivalent circuit and the resonant modes of the RSLR are also discussed in detail. By controlling its structure parameters, such as the electrical length ratio and impedance ratio, the tunable stopband region can be obtained. In section IV, the design procedure of a novel dual-band bandpass filter with narrow and wide passband simultaneously and with a wide stopband is shown. The geometrical structure of the proposed dual-band bandpass filter is shown in Figure 1. It is composed by one SIRLR, and a pair of RSLR. In this design, three transmission zeros are provided near the passband edge to enhance the passband selectivity with a sharp cutoff skirt. The designed filter was fabricated and measured. The simulated and measured results are found to be in good agreement. In section V, a conclusion is made to address the advantages and new finding of this design.

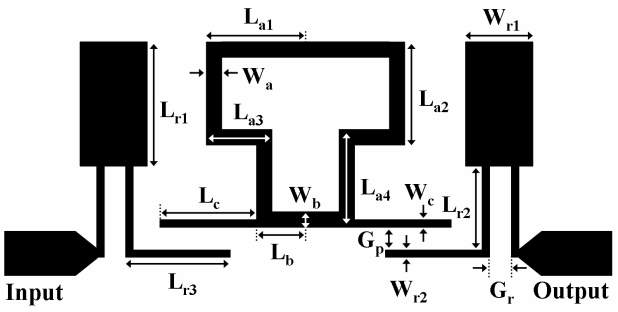

FIGURE 1. Geometrical structure of the proposed dual-band bandpass filter. (Dimensions: L_{a1} = 16.3 mm, L_{a2} = 4.8 mm, L_{a3} = 12.6 mm, L_{a4} = 0.4 mm, L_b = 4.8 mm, L_c = 15.3 mm, W_a = 0.8 mm, W_b = 0.8 mm, W_c = 0.5 mm, G_p = 0.2 mm, L_{r1} = 4.3 mm, L_{r2} = 3.9 mm, L_{r3} = 14.3 mm, W_{r1} = 2.6 mm, W_{r2} = 0.2 mm, and G_r = 0.2mm.

II. DUAL-BAND DESIGN

A. EQUIVALENT CIRCUIT

The SIRLR is applied to excite multiple modes which are used to form the required passband. The SIRLR consists of a ring microstrip line and two open-end microstrip stubs. These two open-end microstrip stubs, having a characteristic admittance of Y_c and an electrical length of θ_c, are tapped on the ring microstrip line. The ring microstrip line has two sections with electrical lengths of θ_a and θ_b, respectively, and with the same characteristic admittance Y_a, as shown in Figure 2(a). Due to the symmetrical structure, even- and odd-mode analysis is used to analyze the resonant characteristic of the SIRLR. The even- and odd-mode equivalent circuits of the proposed SIRLR are shown as Figure 2(b).

For even-mode excitation, the symmetrical plane shown in Figure 2(a) behaves as a magnetic wall (M.W.) and is thus considered as an open-circuited end. The input admittance (Y_{ine}) of this even-mode equivalent circuit is derived as follows:

$$Y_{ims} = jY_c \frac{Y_a \tan\theta_a + Y_a \tan\theta_b + Y_c \tan\theta_c}{Y_c - Y_a(\tan\theta_c \tan\theta_a + \tan\theta_c \tan\theta_b)} \quad (1a)$$

In contrast, for odd-mode excitation, the symmetrical plane shown in Figure 2(a) behaves as an electric wall (E.W.) and is considered as a short-circuited end. The input admittance (Y_{ino}) of this odd-mode equivalent circuit is derived as follows:

$$Y_{ino} = jY_c \frac{-Y_a \cot\theta_a - Y_a \cot\theta_b + Y_c \tan\theta_c}{Y_c - Y_a(\tan\theta_c \cot\theta_a + \tan\theta_c \cot\theta_b)} \quad (1b)$$

In addition, in order to control the resonant modes (even- and odd-mode) simply, the structure parameters of the

$$Y_{ine} = jY_c \frac{K\left[\tan\left(\theta_T \cdot \alpha\right) + \tan\left(\theta_T - \gamma\right)\right] + \tan\left(\theta_T \cdot (1-\alpha)\right)}{1 - K\left[\tan\left(\theta_T \cdot (1-\alpha)\right)\tan\left(\theta_T \cdot \alpha\right) + \tan\left(\theta_T \cdot (1-\alpha)\right)\tan\left(\theta_T \cdot \gamma\right)\right]} \tag{2a}$$

$$Y_{ino} = jY_c \frac{-K\left[\cot\left(\theta_T \cdot \alpha\right) + \cot\left(\theta_T \cdot \gamma\right)\right] + \tan\left(\theta_T \cdot (1-\alpha)\right)}{1 + K\left[\tan\left(\theta_T \cdot (1-\alpha)\right)\cot\left(\theta_T \cdot \alpha\right) + \tan\left(\theta_T \cdot (1-\alpha)\right)\cot\left(\theta_T \cdot \gamma\right)\right]} \tag{2b}$$

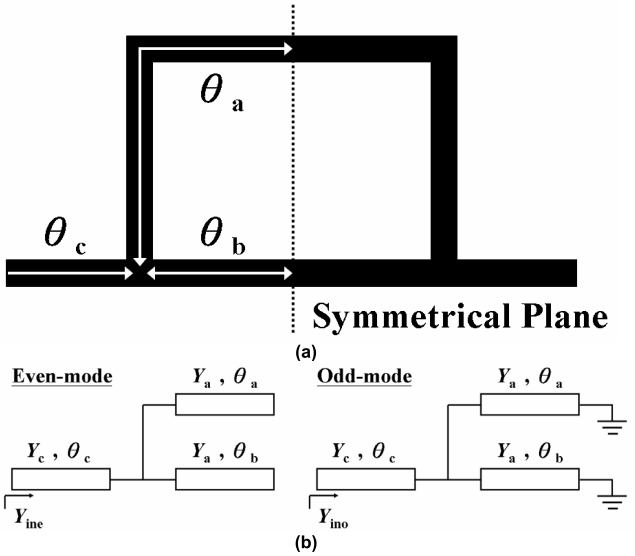

FIGURE 2. (a) Basic structure and (b) even- and odd-mode equivalent circuits of the proposed SIRLR.

proposed SIRLR (θ_a, θ_b, θ_c, Y_a, and Y_c) are replaced by three parameters (α, γ, and K). The first electrical length ratio is expressed as $\alpha = \theta_a/(\theta_a + \theta_c) = \theta_a/\theta_T$, the second electrical length ratio is expressed as $\gamma = \theta_b/(\theta_a + \theta_c) = \theta_b/\theta_T$, and the admittance ratio is expressed as $K = Y_a/Y_c$. Therefore, (1a) and (1b) can be rewritten as (2a) and (2b), as shown at the top of this page.

Based on (2a) and (2b), the resonant modes can be excited when the corresponding imaginary admittance is equal to zero (Im $[Y_{ine}] = 0$ or Im $[Y_{ino}] = 0$) [16]. Accordingly, each resonant mode can be tuned by varying the three parameters (α, γ, and K). The calculated resonant electrical length of each mode versus α and different K using MATLAB tool is plotted in Figure 3.

Figure 3(a) illustrates the resonant electrical length of each mode with a fixed value of $\gamma = 0.1$. Obviously, the difference between the relative even- and odd-mode shows an irregular trend. For the first two modes (f_{o1} and f_{e1}), the first even-mode (f_{e1}) and the first odd-mode (f_{o1}) become closer mutually when the electrical length ratio (α) is increased from 0 to 0.6. In contrast, when α is increased from 0.6 to 1, the first even-mode (f_{e1}) and the first odd-mode (f_{o1}) shift apart from each other. For the second two modes (f_{o2} and f_{e2}), the second even-mode (f_{e2}) and the second odd-mode (f_{o2}) become closed mutually when α is increased from 0 to 0.4 and from 0.7 to 1.0. In contrast, when α is increased from 0.4 to 0.7, the second even-mode (f_{e2}) and the second odd-mode (f_{o2}) shift apart from each other. Figure 3(b) and Figure 3(c) illustrates the resonant electrical length of each mode with different values of $\gamma = 0.2$ and 0.3, respectively. Similarly, each mode can be tuned to meet the required resonant characteristic of the SIRLR by varying α and K.

In this design, the first even-mode (f_{e1}) and the first odd-mode (f_{o1}) are excited to form the first passband, and the second even-mode (f_{e2}) and the second odd-mode (f_{o2}) are excited to form the second passband. To further simplify the design procedure of deciding the structure parameters, a normalized frequency ratio (f_R) is defined as:

$$f_R = \frac{f_{p2}}{f_{p1}} = \frac{|f_{e2} - f_{o2}|/2}{|f_{e1} - f_{o1}|/2} \tag{3}$$

where f_{p1} represents the center frequency of the first passband, and f_{p2} represents the center frequency of the second passband. The calculated normalized frequency ratio (f_R) versus α and different K using MATLAB tool is plotted in Figure 4. Accordingly, the normalized frequency ratio can be calculated in accordance with the required f_{p1} and f_{p2} to find proper values of α and K from Figure 4. In addition, a proper value of γ could be obtained from Figure 3 based on the required bandwidth of the two passbands.

To clarify the resonant characteristics of the SIRLR, a design example of the SIRLR, having a narrow passband at 2.4 GHz and a wide passband at 4 GHz (over a bandwidth range from 3 to 5 GHz), is presented as follows. The normalized frequency ratio can be calculated as $f_R = 1.67$ due to $f_{p1} = 2.4$ GHz and $f_{p2} = 4$ GHz. As presented in Figure 4, there are six cases of (α, γ, and K) that satisfy the requirement of $f_R = 1.67$, including: (0.7, 0.1, 1.25), (0.6, 0.1, 1.25), (0.65, 0.2, 1.25), (0.55, 0.2, 1.25), (0.62, 0.3, 1.25), and (0.48, 0.3, 1.25). However, for the demand of wider bandwidth, the difference between f_{e2} and f_{o2} should be larger than the difference between f_{e1} and f_{o1}. Therefore, a proper value of $\gamma = 0.1$ could be determined from Figure 3. Consequently, the most proper values of (α, γ, and K) are chosen as (0.7, 0.1, 1.25), and the relative structure parameters of the SIRLR are decided as $\theta_a = 120°$, $\theta_b = 17°$, $\theta_c = 50°$, $1/Y_a = 95\Omega$, and $1/Y_c = 115\Omega$ with corresponding physical dimensions of $L_a = 34.1$ mm, $L_b = 4.8$ mm, $L_c = 15.3$ mm, $W_a = 0.8$ mm, $W_b = 0.8$ mm, and $W_c = 0.5$ mm, respectively.

B. RESONANT CHARACTERISTIC

To further explore the frequency response of the SIRLR, the proposed example of the SIRLR, having given physical dimensions as discussed in Section II. (A), is simulated by using Zeland IE3D full wave electromagnetic (EM) simulator [13]. In Figure 5(a), four resonant modes (f_{e1}, f_{o1}, f_{e2}, and f_{o2}) are excited at 2.3, 2.6, 3.5, and 4.3 GHz in a

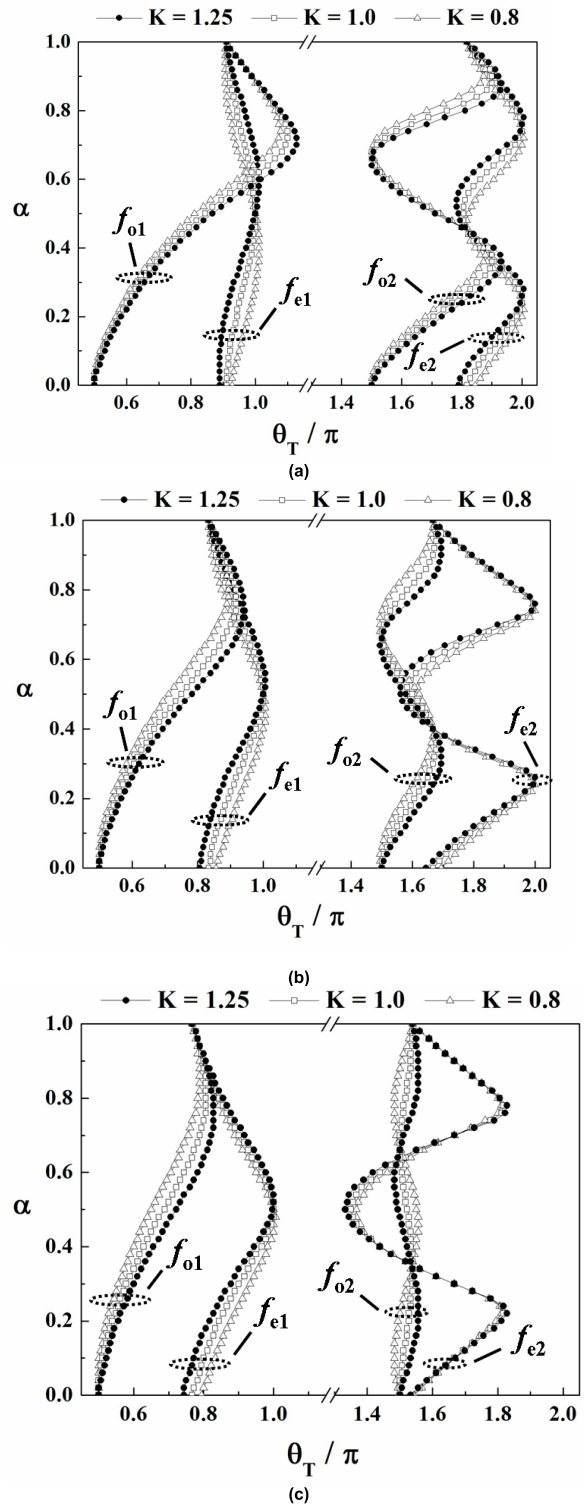

FIGURE 3. Calculated resonant electrical length of each mode versus electrical length ratio (α) with different impedance ratios (K = 1.25, 1.0, and 0.8) by fixing the value of electrical length ratio (γ) at (a) 0.1, (b) 0.2 and (b) 0.3 using MATLAB tool.

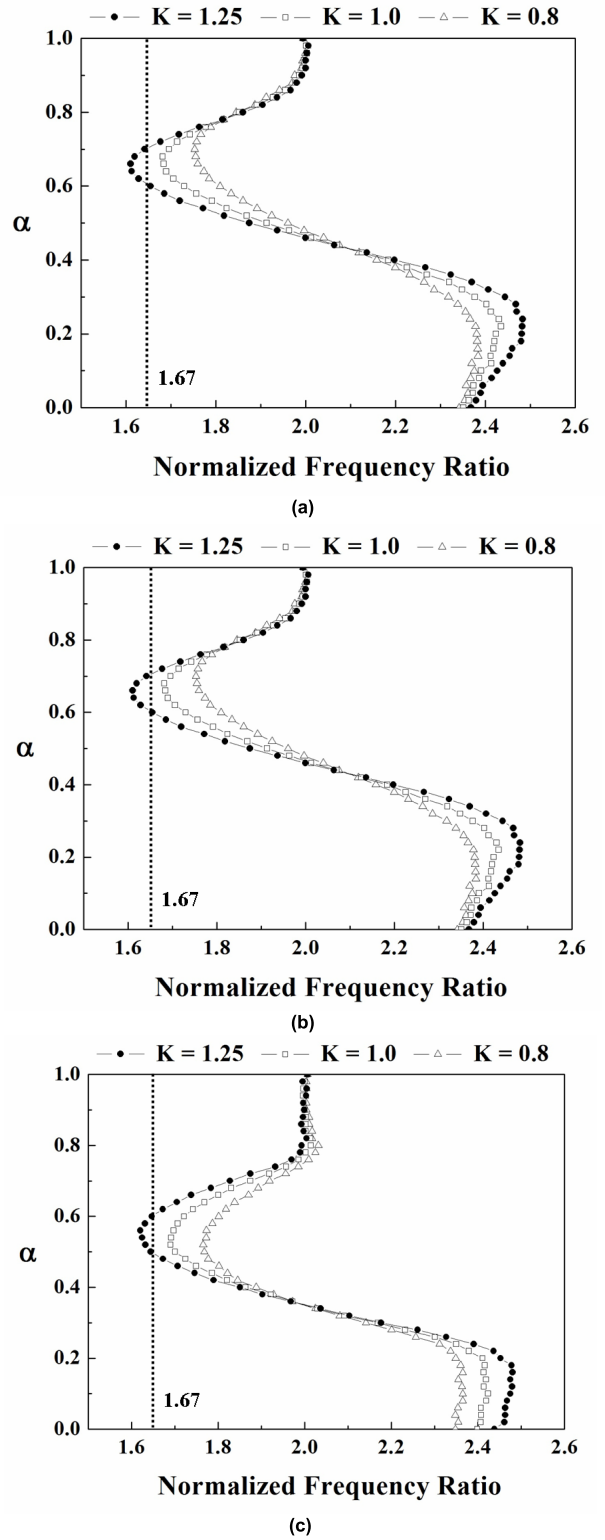

FIGURE 4. Calculated normalized frequency ratio versus electrical length ratio (α) with different impedance ratios (K = 1.25, 1.0, and 0.8) by fixing the value of electrical length ratio (γ) at (a) 0.1, (b) 0.2 and (b) 0.3 using MATLAB tool.

weak coupling condition using EM simulation, respectively. These four resonant modes are used to form a narrow passband at 2.4 GHz and a wide passband at 4 GHz with a bandwidth range from 3 to 5 GHz. It is also noted that the third even-mode (f_{e3}) and the third odd-mode (f_{o3}), excited at 5.7 and 5.9 GHz, are regarded as spurious response and

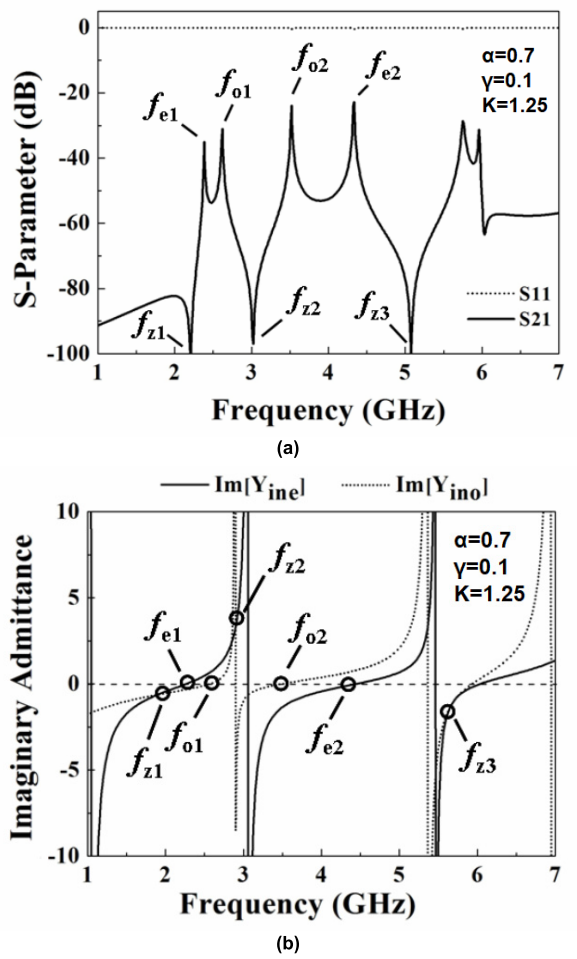

FIGURE 5. (a) Simulated resonant modes in a weak coupling condition using EM simulation and (b) calculated imaginary admittance using MATLAB tool of odd- and even-mode ($\mathrm{Im}[Y_{\mathrm{ino}}]$ and $\mathrm{Im}[Y_{\mathrm{ine}}]$) for the proposed SIRLR with $\alpha = 0.7$, $\gamma = 0.1$, and K = 1.25.

should be suppressed in this design (as will be discussed in the Section III).

Moreover, three transmission zeros ($\mathrm{TZ_{p1}}$, $\mathrm{TZ_{p2}}$, and $\mathrm{TZ_{p3}}$) are created near the passband edge at frequencies (f_{z1}, f_{z2}, and f_{z3}) of 2.2, 3.0, and 5.1 GHz, thus improving the passband selectivity. The location of transmission zero can also be controlled by analyzing the transfer function of the proposed SIRLR. Based on (2) and with $\alpha = 0.7$, $\gamma = 0.1$ and $K = 1.25$, the calculated values of the imaginary admittance of even- and odd-mode versus frequency using MATLAB tool are plotted in Figure 5(b). As discussed in Section II. (A), resonant modes (f_e and f_o) are excited corresponding to the resonant condition of $\mathrm{Im}[Y_{\mathrm{ine}}] = 0$ or $\mathrm{Im}[Y_{\mathrm{ino}}] = 0$. Therefore, the transfer function of symmetrical two-port networks can be expressed as [16]:

$$S_{21} = \frac{Y_0 Y_{ino} - Y_0 Y_{ins}}{(Y_0 + Y_{ino})(Y_0 + Y_{ins})} = \frac{Y_{ino}}{Y_0 + Y_{ino}} - \frac{Y_{ins}}{Y_0 + Y_{inc}} \tag{4}$$

The condition of transmission zeros can be obtained as setting $|S_{21}| = 0$. Accordingly, the transmission zeros of the proposed SIRLR are achieved as $\mathrm{Im}[Y_{\mathrm{ine}}] = \mathrm{Im}[Y_{\mathrm{ino}}]$ (cross point in Figure 5(b)). It is verified that the calculated results in Figure 5(b) are in good agreement with the simulated results in Figure 5(a).

C. MODE EXTENSION

For the demand of wideband response, additional modes shall be provided to obtain a flat passband response. In this design, two identical microstrip lines are connected at the I/O ports and used to couple with the SIRLR as shown in Figure 6(a). Each coupled section is considered as a J-inverter with two equivalent transmission lines ($\theta_{r3}/2$).

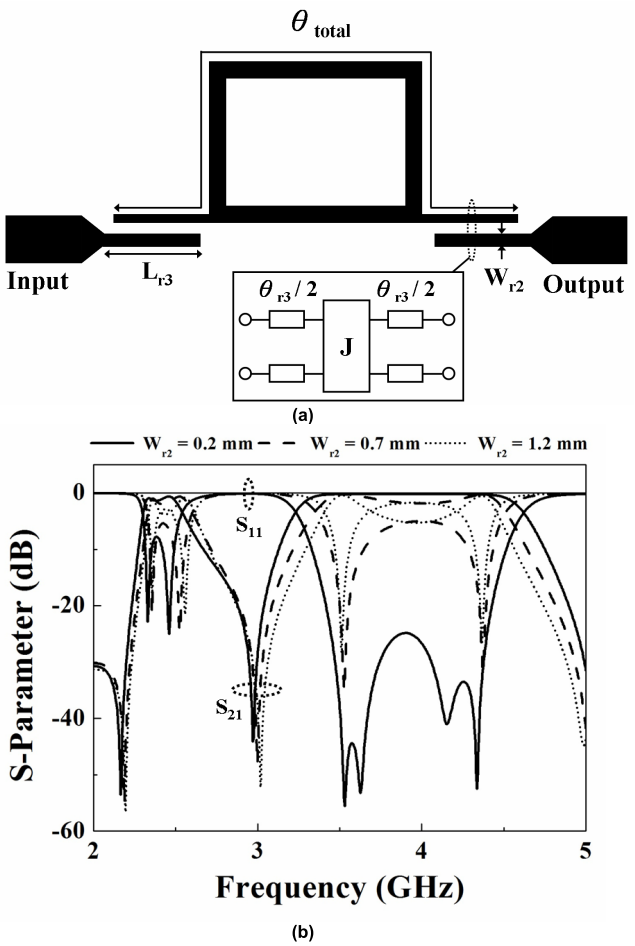

FIGURE 6. (a) Layout and (b) S-parameter of the proposed SIRLR with two coupled I/O ports.

To further observe the coupling behavior between the SIRLR and the microstrip lines, a total electrical length (θ_{total}) for the SIRLR is defined to analyze and the return loss ($|S_{11}|$). Based on the transmission line theory [18], [19], the return loss for the whole circuit, including SIRLR and two coupled microstrip lines, can be expressed as:

$$S_{11} = \frac{j \tan\theta_{\mathrm{tranl}} \cdot \left(1 - \bar{J}^4\right)}{2\bar{J}^2 + j \tan\theta_{\mathrm{total}} \cdot \left(1 + \bar{J}^4\right)} \tag{5}$$

where $\bar{J}$ is the normalized susceptance of the J-inverter and it is equal to J/Y_{r2}. Based on (5), the resonant conditions of each

mode ($|S_{11}| = 0$) are obtained in the two cases as $tan(\theta_{\text{total}}) = 0$ and $\bar{J} = 1$. It shall be noted that the case of $tan(\theta_{\text{total}}) = 0$ occurs in accordance with the resonance of the SIRLR, therefore, all resonant modes (f_e and f_o) are remained after adding two coupled microstrip lines. Furthermore, additional modes, used to obtain the required flat passband response, are created by satisfying the case of $\bar{J} = 1$. Therefore, a flat passband response can be realized by enhancing the coupling energy between the SIRLR and the microstrip lines as shown in FIGURE 6(b). When the width of the microstrip line (W_{r2}) is reduced from 1.2 mm to 0.2 mm, two additional poles are created at 3.6 and 4.1 GHz that improves the flatness of the passband.

Based on the above analysis, we designed a dual-band bandpass filter, having a narrow-band and wide-band response, as shown in Figure 7(a). After optimizing, the physical dimensions of hits dual-band bandpass filter were chosen as: $L_a = 34.1$ mm, $L_b = 4.8$ mm, $L_c = 15.3$ mm, $L_{r3} = 14.3$ mm, $W_a = 0.8$ mm, $W_b = 0.8$ mm, $W_c = 0.5$ mm, and $W_{r2} = 0.2$ mm, respectively. Figure 7(b) shows the simulated results of the proposed dual-band bandpass filter. It shows good performance for both the narrow and wide passband. However, an undesired interference, which is created due to spurious response of the SIRLR, occurs from 5 GHz to 20 GHz and should be suppressed.

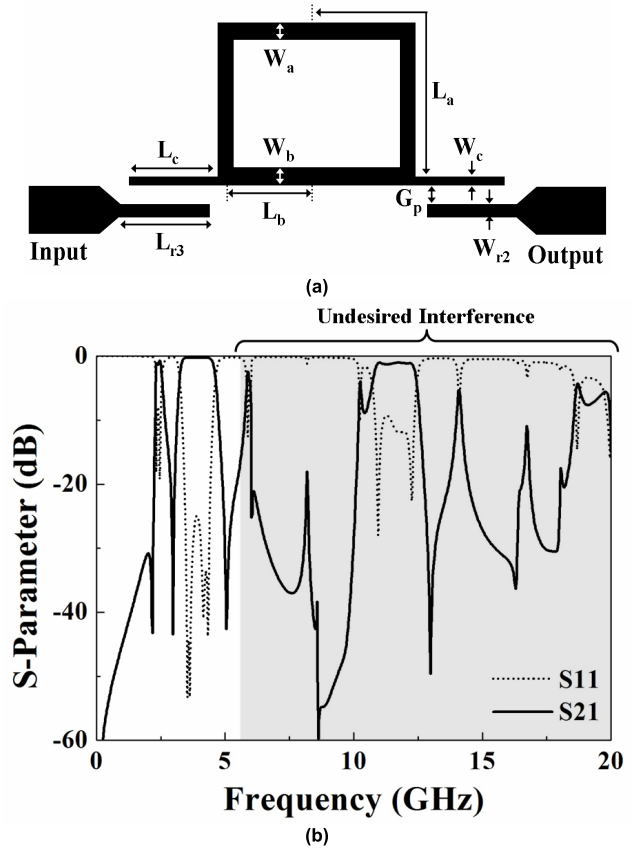

FIGURE 7. (a) Geometrical structure and (b) simulated results of the proposed dual-band bandpass filter with undesired interference.

III. WIDE STOPBNAD DESIGN

As discussed in Section II, the spurious response of the proposed SIRLR, located at 5.7 and 5.9 GHz, shall be suppressed to improve the performance of the designed dual-band bandpass filter. However, not only two spurious responses but also undesired interference, located at high-frequency side (from 6 to 20 GHz) as shown in Figure 7, shall be improved. By considering various types of low pass filter or bandstop filter, a low-pass resonator, which can provide multiple transmission zeros and wide stopband region, is better than a bandstop filter, typically having a narrow stopband region.

In this design, we adopted the designed rectangular stub loaded resonator (RSLR), as shown in Figure 8(a), to execute the low pass function [20] since it is easy to tune the extensive stopband region by controlling its several structure parameters. It consists of a rectangular stub patch and a parallel coupled line in a symmetrical structure.

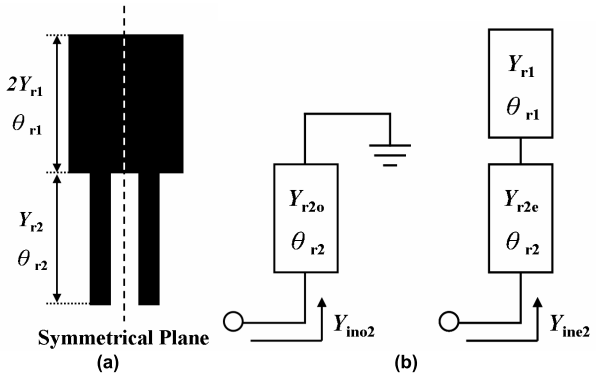

FIGURE 8. (a) Layout and (b) odd- and even- mode equivalent circuits of the used rectangular stub loaded resonator (RSLR).

A. EQUIVALENT CIRCUIT

The characteristic admittance and electrical length of the rectangular stub patch and the parallel coupled line are defined as $(2Y_{r1}, \theta_{r1})$ and (Y_{r2}, θ_{r2}), respectively. By using even- and odd-mode analysis again, two equivalent circuits with an open-circuited plane and a short-circuited plane (for the even- and odd-mode, respectively) are built as shown in Figure 8(b). Herein, the characteristic admittances of the parallel coupled line for the even- and odd-mode are determined as Y_{r2e} and Y_{r2o}. Based on these equivalent circuits (even- and odd-mode), the input admittances looking into the parallel coupled line (Y_{ino2} and Y_{ine2}) are expressed as follows:

$$Y_{ino2} = -jY_{r2o}\cot\theta_{r2} \tag{6a}$$

$$Y_{ine2} = -jY_{r2e}\frac{Y_{r1}\tan\theta_{r1} + Y_{r2e}\tan\theta_{r2}}{Y_{r1}\tan\theta_{r1}\tan\theta_{r2} - Y_{r2e}} \tag{6b}$$

where Y_{r2o} and Y_{r2e} are the odd- and even-mode characteristic impedances of the parallel coupled line, respectively. In addition, the occurring condition of the transmission zeros ($S_{21} = 0$) are derived as $\text{Im}[Y_{ino2}] = \text{Im}[Y_{ine2}]$ based on (4). In the past, an electrical length ratio was used to adjust the location of the transmission zeros [21], [22]. However,

the tuning ability of the transmission zero is less when only using the electrical length ratio and thus the ultra wide stopband region can not achieved easily. Therefore, we further defined a novel impedance ratio ($R = Z_{r1}/Z_{r2e} = Y_{r2e}/Y_{r1}$) into (6) to tune the transmission zeros instead of merely using the electrical length ratio ($\beta = \theta_{r1}/\theta_{r2}$). Thus, the input admittance of the even-mode can be rewritten as:

$$Y_{ine2} = -jY_{r2e}\frac{\tan(\beta\theta_{r2}) + R\tan\theta_{r2}}{\tan(\beta\theta_{r2})\tan\theta_{r2} - R} \tag{7}$$

In this design, the characteristic parameters of the parallel coupled line are given as: $Z_{r2o} = 1/Y_{r2o} = 94$ Ohms, $Z_{r2e} = 1/Y_{r2e} = 220$ Ohms, and $\theta_{r2} = 45°$. It is noted that the characteristic parameters of the rectangular stub patch (Z_{r1} and θ_{r1}) is regarded as core parameters for varying the determined ratios (R and β).

B. RESONANT CHARACTERISTIC

To observe the varied range of the transmission zeros, the calculated values of imaginary admittance of even- and odd-mode versus frequency as function of R and βusing MATLAB tool, are plotted in Figure 9(a) and Figure 10(a), respectively.

It is clearly observed that the designed RSLR generates three transmission zeros (f_{r1}, f_{r2}, and f_{r3}) when the value of electrical length ratio (β) is tuned under the range from 0.9 to 1.1. In accordance with the required region of the stopband, f_{r2} can be tuned to approach f_{r1} by increasing β or f_{r3} by decreasing β. However, if β is chosen lower than 0.7 or higher than 1.3, the second transmission zero (f_{r2}) will disappear and cause poor interference suppression. The simulated frequency responses with varied values of β are shown in Figure 9(b) and exhibit a good agreement with the calculated results.

In Figure 10(a), we varied the impedance ratio (R) to control the transmission zeros with a fixed $\beta = 1.1$. By decreasing the value of R, the first transmission zero (f_{r1}) and third transmission zero (f_{r3}) are shifted toward lower- and higher-frequency side respectively without affecting the second

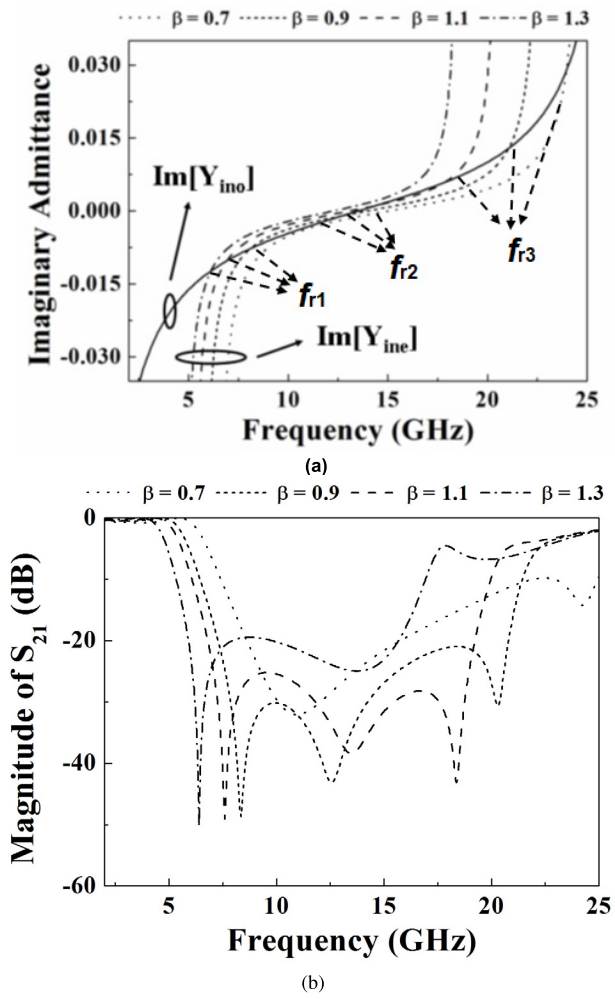

FIGURE 9. (a) Calculated imaginary admittance of odd- and even-mode ($\mathrm{Im}[Y_{ino}]$ and $\mathrm{Im}[Y_{ine}]$) using MATLAB tool and (b) simulated results for the proposed RSLR with different values of β. ($Z_{r2o} = 94$ Ohms, $Z_{r2e} = 220$ Ohms, $\theta_{r2} = 45°$, and $R = 0.4$).

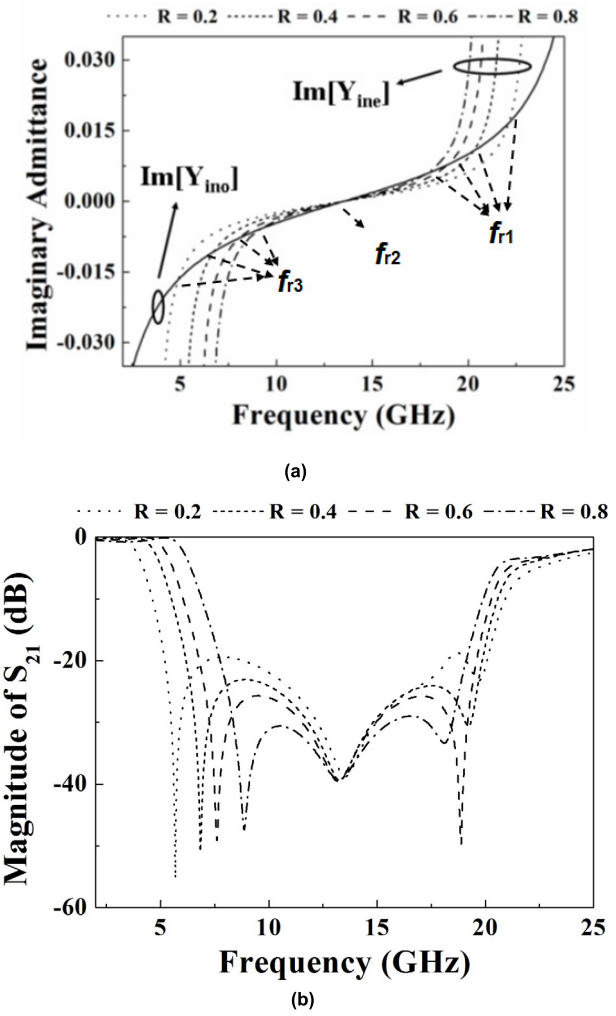

FIGURE 10. (a) Calculated imaginary admittance of odd- and even-mode ($\mathrm{Im}[Y_{ino}]$ and $\mathrm{Im}[Y_{ine}]$) using MATLAB tool and (b) simulated results for the proposed RSLR with different values of R. ($Z_{r2o} = 94$ Ohms, $Z_{r2e} = 220$ Ohms, $\theta_{r2} = 45°$, and $\beta = 1.1$).

TABLE 1. Performance comparison of this work with other dual-band bandpass filter.

Ref.	Passbands (GHz)	Passband Bandwidth	Insertion Loss (dB)	FBW (%)	Resonators	Stopband (GHz)	Size (λ_g x λ_g)
[2]	1.45/2.02	Narrow/ Narrow	0.9/1.3	8.5/7.9	2	(X)	0.25 x 0.25
[3]	2.35/3.15	Narrow/ Narrow	0.5/1.5	4/3	4	(X)	0.19 x 0.2
[4]	2.4/5.2	Narrow/ Narrow	0.4/0.58	20/10	2	6 ~ 9	0.25 x 0.22
[5]	2.4/5.2	Narrow/ Narrow	0.42/0.91	14.2/12	3	(X)	0.28 x 0.24
[6]	2.4/5.2	Narrow/ Narrow	0.42/0.7	24/14	2	(X)	0.22 x 0.11
[7]	1.8/3.9	Narrow/ Wide	0.62/0.35	14/46	2	(X)	0.28 x 0.34
[8]	0.61/1.35	Narrow/ Narrow	0.45/0.75	32.3/10.5	2	(X)	0.44 x 0.03
[9]	2.45/5.85	Narrow/ Narrow	0.06/2.04	32.3/10.5	2	(X)	(X)
[10]	1.57/2.38	Narrow/ Narrow	1.21/1.95	9.9/6.5	2	(X)	1.1 x 0.48
[11]	1.84/2.9	Narrow/ Narrow	1.7/1.6	8.1/6.8	2	(X)	0.32 x 0.14
[12]	1.57/2.45	Narrow/ Narrow	1.26/2.4	9/8.5	1	2.5 ~ 5	0.09 x 0.12
[13]	2.3/4.1	Narrow/ Narrow	0.65/1	19/11	1	4.9 ~ 7.3	0.37 x 0.37
[14]	0.9/2.25	Narrow/ Narrow	0.5/1.0	6.4/4.4	1	(X)	0.28 x 0.23
This work	2.4/4	Narrow/Wide	1.4/1	8/39	2	5 ~ 20	0.48 x 0.09

transmission zero (f_{r2}), thus extending the stopband region. The simulated frequency responses with varied values of R are shown in Figure 10(b) and also exhibit a good agreement with the calculated results.

Figure 11 shows the calculated and simulated results of the designed RSLR. For the demand of stopband region from 6 to 20 GHz, the RSLR provided three transmission zeros (TZ_1, TZ_2 and TZ_3) of $f_{r1}/f_{r2}/f_{r3}$ at 7.0/13.4/18.4 GHz respectively when the parameters of the RSLR are determined as $\beta = 1.1$ and $R = 0.4$. Consequently, the physical dimensions of the RSLR are decided as: $W_{r1} = 2.6$ mm, $L_{r1} = 4.3$ mm, $W_{r2} = 0.2$ mm, $L_{r2} = 3.9$ mm, and $G_r = 0.2$mm, respectively.

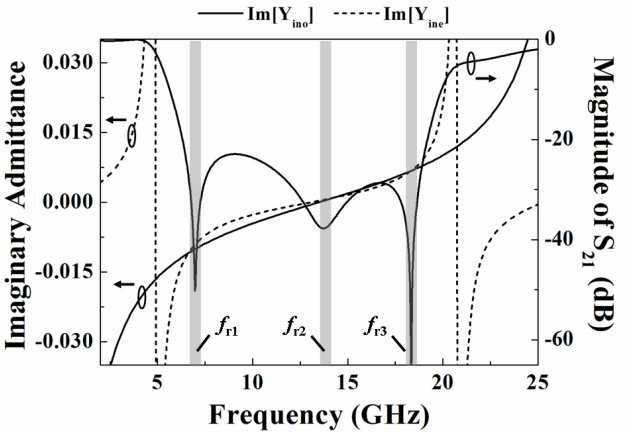

FIGURE 11. Calculated imaginary admittance and simulated results for the designed RSLR. ($Z_{r2o} = 94$ Ohms, $Z_{r2e} = 220$ Ohms, $\theta_{r2} = 45°$, $R = 0.4$ and $\beta = 1.1$).

C. COMBINATION OF SIRLR AND RSLR

In this design, the RSLRs, used to suppress undesired spurious responses of the SIRLR, are attached between the identical microstrip lines (discussed in Section II (C)) and the I/O ports as shown in Figure 1. By locating the transmission zeros at proper frequencies, the proposed dual-band bandpass filter provides a broad stopband region as shown in Figure 12. After attaching the RSLRs, the proposed dual-band bandpass filter shows good performance, including low insertion loss of 0.66 dB at the first passband and 0.5 dB at the second passband, and wide stopband region from 5 to 20 GHz with a rejection level of 25 dB.

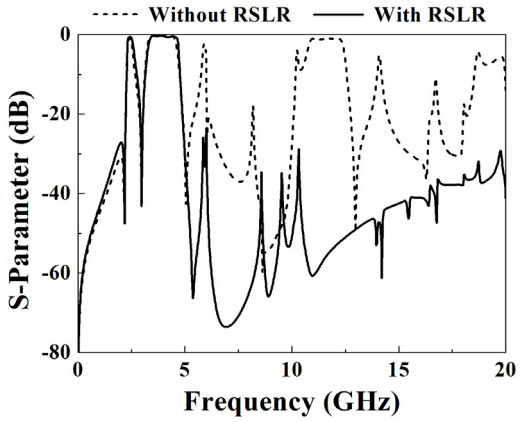

FIGURE 12. Comparison of the simulated S_{21} results of the proposed dual-band bandpass filter with/without the RSLR.

IV. EXPERIMENT RESULT AND DISSCUSION

In order to verify the proposed concept, the filter example is designed based on the following procedure:

1. Decide the required band performances such as center frequencies, bandwidth, stopband region;
2. Determine the resonant modes of the SIRLR to satisfy the required passband by carefully choosing the electrical length ratio and impedance ratio of the SIRLR;
3. Adopt microstrip lines to couple with the SIRLR for the required bandwidth'
4. Determine the transmission zeros of the RSLR to achieve the enough wide stopband by probably choosing the electrical length ratio and impedance ratio of the RSLR;
5. Combine the SIRLR with the RSLR taped at the input/output ports of the SIRLR.

The designed dual-band bandpass filter was fabricated on RT/Duroid 5880 substrate and measured by an HP8510C Network Analyzer. The given parameters of RT/Duroid 5880 substrate includes a relative dielectric constant of 2.2, a loss tangent of 0.0009 and a thickness of 0.787 mm. Figure 13(a) shows the fabricated dual-band bandpass filter. The whole circuit size of this filter is 44.6 mm × 8.2 mm, approximately $0.48\lambda_g \times 0.09\lambda_g$ (not includes I/O ports), and λ_g is the guided wavelength of the 50Ω transmission line at the fundamental frequency ($f_0 = 2.4$ GHz) of the SIRLR. It is noted that the SIRLR was bent to obtain a minimal circuit size with a slight and negligible influence for the passband responses.

Figure 13(b) shows the measured S_{21} and S_{11} results of the fabricated dual-band bandpass filter. To observe the measured results clearly, a zoom plot for the passband responses was shown in Figure 13(c). For the narrow passband, the measured performances include a center frequency at 2.4 GHz, a low insertion loss of 1.4 dB, band selectivity of 370 dB/GHz at the lower edge and 62.5 dB/GHz at the upper edge, and a fractional bandwidth (FBW) of 8%. For the wide passband, the measured performances include a center frequency at

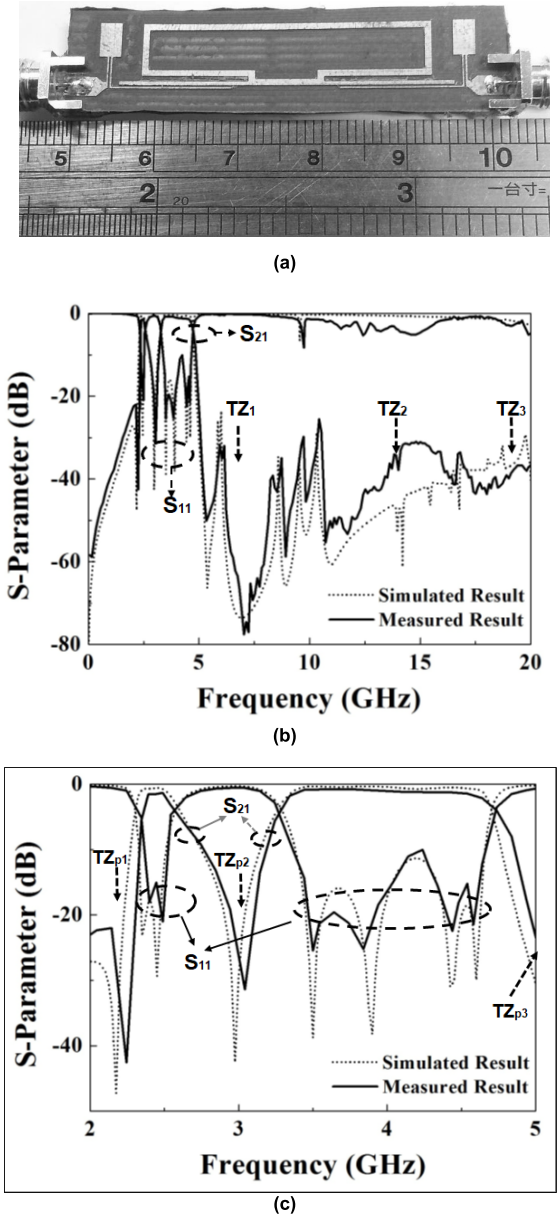

FIGURE 13. (a) Photograph and (b) simulated/measured S_{21} and S_{11} results of the designed dual-band bandpass filter. (c) Zoom plot for the passband responses.

4.0 GHz, a low insertion loss of 1.0 dB around the passband, band selectivity of 128.2 dB/GHz at the lower edge and 94 dB/GHz at the upper edge, and a fractional bandwidth (FBW) of 39%. Three transmission zeros near the passbands (TZ_{p1}, TZ_{p2} and TZ_{p3}) and three transmission zeros (TZ_1, TZ_2 and TZ_3) in the stopband are clearly observed in the measured results.

Table 1 compares the performance of the proposed design with the other reported dual-band bandpass filter. It is noted that less researches design a dual-band bandpass filter with simultaneous narrow- and wide-bandwidth. In addition, most researches do not consider the stopband response within high frequency region. However, we presented a dual-band

bandpass filter with narrow and wide passband simultaneously as well as a wide stopband. By attaching the proposed RSLRs, moreover, the unwanted spurious responses of the SIRLR were suppressed effectively; moreover, a wide stopband region was accomplished from 5 to 20 GHz with a rejection level of 25 dB.

V. CONCLUSION

A dual-band bandpass filter with narrow-band and wide-band performances has been proposed in this paper. Only one SIRLR is used to achieve the dual-band response. Based on the proposed equivalent circuit, each mode of the SIRLR (even- and odd-mode) can be controlled according to different electrical length ratios (α and γ) and admittance ratio (K). Moreover, multi transmission zeros are created near each passband edge, thus improving the passband selectivity. To extend the stopband region, a pair of RSLR is added into the filter to suppress effectively the undesired spurious response. Finally, the designed dual-band bandpass filter are fabricated and measured, and the measured results match the theoretical prediction. This designed dual-band filter has a narrow passband at 2.4 GHz with bandwidth ratio of 8% and a wide passband from 3 to 5 GHz, which can be used in the wireless communications applications, such as IEEE 802.11 wireless local area networks (WLANs) and ultra-wide band (UWB) system.

REFERENCES

[1] L.-C. Tsai and C.-W. Hsue, "Dual-band bandpass filters using equal-length coupled-serial-shunted lines and Z-transform technique," *IEEE Trans. Microw. Theory Techn.*, vol. 52, no. 4, pp. 1111–1117, Apr. 2004.

[2] X. Y. Zhang and Q. Xue, "Novel dual-mode dual-band filters using coplanar-waveguide-fed ring resonators," *IEEE Trans. Microw. Theory Techn.*, vol. 55, no. 10, pp. 2183–2190, Oct. 2007.

[3] B. Wu, C. H. Liang, Q. Li, and P. Y. Qin, "Novel dual-band filter incorporating defected sir and microstrip SIR," *IEEE Microw. Wireless Compon. Lett.*, vol. 18, no. 6, pp. 392–394, Jun. 2008.

[4] H.-W. Wu, Y.-F. Chen, and Y.-W. Chen, "Multi-layered dual-band bandpass filter using stub-loaded stepped-impedance and uniform-impedance resonators," *IEEE Microw. Wireless Compon. Lett.*, vol. 22, no. 3, pp. 114–116, Mar. 2012.

[5] Y. P. Zhang and M. Sun, "Dual-band microstrip bandpass filter using stepped-impedance resonators with new coupling schemes," *IEEE Trans. Microw. Theory Techn.*, vol. 54, no. 10, pp. 3779–3785, Oct. 2006.

[6] M. H. Weng, H. W. Wu, and Y. K. Su, "Compact and low loss dual-band bandpass filter using pseudo-interdigital stepped impedance resonators for WLANs," *IEEE Microw. Wireless Compon. Lett.*, vol. 17, no. 3, pp. 187–189, Mar. 2007.

[7] C.-Y. Huang, M.-H. Weng, C.-Y. Hung, and S.-W. Lan, "Design of a dual-band bandpass filter for GSM and direct sequence ultra-wideband communication systems," *J. Electromagn. Waves Appl.*, vol. 25, pp. 1605–1615, Jun. 2011.

[8] R. Zhang and L. Zhu, "Design of a compact dual-band bandpass filter using coupled stepped-impedance resonators," *IEEE Microw. Wireless Compon. Lett.*, vol. 24, no. 3, pp. 155–157, Mar. 2014.

[9] J.-X. Chen, M.-Z. Du, Y.-L. Li, Y.-J. Yang, and J. Shi, "Independently tunable/controllable differential dual-band bandpass filters using element-loaded stepped-impedance resonators," *IEEE Trans. Compon., Packag., Manuf. Technol.*, vol. 8, no. 1, pp. 113–120, Jan. 2018.

[10] R. Gómez-García, L. Yang, J.-M. Muñoz-Ferreras, and D. Psychogiou, "Selectivity-enhancement technique for stepped-impedance-resonator dual-passband filters," *IEEE Microw. Wireless Compon. Lett.*, vol. 29, no. 7, pp. 453–455, Jul. 2019.

[11] X. Y. Zhang, J.-X. Chen, Q. Xue, and S.-M. Li, "Dual-band bandpass filters using stub-loaded resonators," *IEEE Microw. Wireless Compon. Lett.*, vol. 17, no. 8, pp. 583–585, Aug. 2007.

[12] Y. Peng, L. Zhang, J. Fu, Y. Wang, and Y. Leng, "Compact dual-band bandpass filter using coupled lines multimode resonator," *IEEE Microw. Wireless Compon. Lett.*, vol. 25, no. 4, pp. 235–237, Apr. 2015.

[13] S. Sun, "A dual-band bandpass filter using a single dual-mode ring resonator," *IEEE Microw. Wireless Compon. Lett.*, vol. 21, no. 6, pp. 298–300, Jun. 2011.

[14] C.-F. Chen, G.-Y. Wang, and J.-J. Li, "Compact microstrip dual-band bandpass filter and quad-channel diplexer based on quint-mode stub-loaded resonators," *IET Microw. Antennas Propag.*, vol. 12, no. 12, pp. 1913–1919, Dec. 2018.

[15] X. Jin, X. Huang, D. Chen, and C. Cheng, "Response diversity of stub-loaded ring bandpass filter based on commensurate line element: Single- and dual-band applications," *IEEE Access*, vol. 7, pp. 25681–25689, 2019.

[16] J.-S. Hong and M. J. Lancaster, *Microstrip Filters for RF / Microwave Applications*. New York, NY, USA: Wiley, 2001.

[17] *IE3D Simulator*, Zeland Software, Fremont, CA, USA, 2002.

[18] L. Zhu, H. Bu, and K. Wu, "Broadband and compact multi-pole microstrip bandpass filters using ground plane aperture technique," *IEE Proc.-Microwaves, Antennas Propag.*, vol. 149, no. 1, pp. 71–77, Feb. 2002.

[19] L. Zhu, H. Bu, and K. Wu, "Aperture compensation technique for innovative design of ultra-broadband microstrip bandpass filter," in *IEEE MTT-S Int. Microw. Symp. Dig.*, vol. 1, Jun. 2000, pp. 315–318.

[20] M.-Y. Hsieh and S.-M. Wang, "Compact and wideband microstrip bandstop filter," *IEEE Microw. Wireless Compon. Lett.*, vol. 15, no. 7, pp. 472–474, Jul. 2005.

[21] C.-Y. Hung, M.-H. Weng, and R.-Y. Yang, "A compact sharp-rejection lowpass filter," *Microw. Opt. Technol. Lett.*, vol. 50, no. 4, pp. 894–896, Apr. 2008.

[22] C.-Y. Hung, M.-H. Weng, and R.-Y. Yang, "A dual-mode bandpass filter with a wide stopband using a controllable bandstop structure," *Microw. Opt. Technol. Lett.*, vol. 50, no. 8, pp. 2214–2216, Aug. 2008.